Nonlinear Optical Signature of Nanostructural Transition in Ionic Liquids

Antonin Pardon, Oriane Bonhomme, Clotilde Gaillard, Pierre-François Brevet, Emmanuel Benichou

Nonlinear Optical Signature of Nanostructural Transition in Ionic Liquids

Antonin Pardon,[1] Oriane Bonhomme,[1] Clotilde Gaillard,[2] Pierre-François Brevet, [1]

Emmanuel Benichou[1]

[1] *Univ Lyon, Université Claude Bernard Lyon 1, CNRS, Institut Lumière Matière, F-69622 Villeurbanne, France.*

[2] *Univ Lyon, Université Claude Bernard Lyon 1, CNRS, Institut de Physique des 2 Infinis, F-69622 Villeurbanne, France.*

Corresponding Author : Prof. Emmanuel Benichou, emmanuel.benichou@univ-lyon1.fr

Abstract :

The homologous series of the ionic liquids 1-alkyl-3-methylimidazolium bis(trifluoromethylsulfonyl)imide, $[C_nC_1im][NTf_2]$ (n=2,4,6,8 and 10) was studied by polarization-resolved second harmonic scattering (SHS). The analysis of the polarization plots clearly demonstrates that the SHS response is dominated by an octupolar contribution. Orientational correlations are observed on the nanometer scale in all the investigated ionic liquids, even for the shortest alkyl chain length. A radial distribution of the nonlinear optical sources is evidenced. A sharp transition from short to longer range correlations occurs between ionic liquids with n=4 and 6, signature of the dominating role taken by the alkyl chains. The SHS technique therefore provides structural observation in liquids at scales well-below the diffraction limit and these findings open new interesting perspectives in the domain.

1. Introduction

Ionic liquids (ILs) are a new class of solvents composed solely of ionic species. They are molten salts that are liquid at relatively low temperatures. ILs have attracted a lot of interest for a multitude of applications over the last 15 years as their ionic components can be chosen according to specific needs, giving them unique and adjustable properties [1-5]. ILs have also been identified as alternative media with lower environmental impact in electrochemical applications[6,7] such as batteries and supercapacitors but also as reaction media in biocatalytic processes involving proteins and enzymes[8]. The tunability of their properties is the result of a wide-ranging and rich arrangement of inter- and intramolecular interactions, for instance Coulombic, dipolar, π-π, solvophobic, van der Waals or hydrogen bonding, established between the charged headgroups and the alkyl chains in a single pure IL [9]. The complex interplay of the different molecular interactions in ILs results in the singular structural organization at the nanoscale both in the bulk phase and at the interface [9-16]. The bulk phase microscopic structure can be observed on different scales. The short-range local order is governed by the Coulombic and Van der Waals interactions between ionic species. Ab Initio and density functional theory have for example predicted the formation of ion pairs [17-19]. The structuration of ILs also occurs on a larger scale. For example, alkylimidazolium-based ILs display long-range organization due to the segregation of alkyl chains and the polar ionic moieties into nonpolar and polar domains, respectively. Structural heterogeneities at nanometer scale has been demonstrated experimentally with small-wide angle X-ray (SWAXS) [15,20-25] and neutron scattering [22,26-29]. For the 1-alkyl-3-methylimidazolium bis(trifluoromethanesulfonyl)imide ILs, indicated as $[C_nC_1im][NTf_2]$ where n is the number of carbon atoms in the alkyl chain, SWAXS experiments have shown that the characteristic size of the nanoscale heterogeneities varies linearly with n [23]. The length of the alkyl chain affects the motion of each ion which is connected with macroscopic

physical properties [30]. However, it remains difficult to observe the existence of nanostructuration for alkyl chain length shorter than butyl (n=4). Optical spectroscopic techniques such as femtosecond optical heterodyne-detected Raman-induced Kerr-effect (OHD-RIKES) spectroscopy, terahertz spectroscopy, dielectric relaxation spectroscopy (DRS), low-frequency Raman and coherent anti-Stokes Raman scattering have also been used to probe IL nano-structuration and their related dynamics [31-38]. Recently, the effect of the structural heterogeneities on the microviscosity of ILs has been studied by time-resolved fluorescence [39]. Self-assembled nanostructures have also been intensively studied by molecular dynamics (MD) simulations [9,11,13,20,29,40-44]. The nonpolar domains formed by the longer alkyl chains interconnect to form sponge-like nanostructures. Transition to the percolation regime occurs with the butyl chain length [40] However, structural transition was not directly observable from experimental measurements even if a recent MD study finely analysing SWAXS data has shown it [42].

In the present work, the ILs nanoscale organization is revealed, even for the shortest alkyl chain length. A structural transition occurring as the alkyl chain length increases is clearly and directly evidenced by a nonlinear optical method, even if the information to be collected is on a scale well below the diffraction limit. In addition, analysis of the results provides the chain length at which this transition occurs. For that, second harmonic scattering (SHS) has been used. This technique is based on the conversion of two photons at the fundamental frequency ω into a single photon at the harmonic frequency 2ω. The second harmonic generation process is particularly well-adapted to study interfaces [14,45,46] but is also recognized as a powerful technique to probe local order in liquids [47,48]. The technique can be applied to measure the second-order hyperpolarizabilities of molecular species diluted in liquid phase [49,50], but also those of pure solvents such as ILs [19,51]. SHS is particularly sensitive to the symmetry of the molecular species [52] and to local structures in ILs such as ion pairs[19].

For correlated assemblies of nonlinear sources, the point-like approximation breaks down and retardation must be considered as well [53,54]. This feature has recently been used to evidence long-range correlations in pure water and their progressive loss in aqueous electrolytes as a function of salt concentration [48]. In this study, we apply SHS resolved in polarization to probe the bulk organization of the homologous ILs series 1-alkyl-3-methylimidazolium bis(trifluoromethylsulfonyl)imide $[C_nC_1im][NTf2]$ with n=2,4,6,8 and 10.

2. Materials and methods

2.1 Materials

The $[C_nC_1im][NTf_2]$ ILs were purchased from Solvionic with a purity higher than 99.9%. All these ILs were used as received and were stored under argon. For the SHS measurements, the different ILs were poured into a quartz cell (Hellma).

2.2 Experimental set-up

The experimental setup has been described in previous studies [48,54]. Briefly, a Ti:Sapphire femtosecond laser is used delivering pulses at a wavelength of 800 nm, of 140 fs length, at a repetition rate of 80 MHz. The beam is gently focused in the cell containing the neat ionic liquid with an X10 magnification objective. The SHS intensity is collected at right angle by a cooled CCD camera coupled to a spectrometer. For the polarization analysis of the SHS intensity, a half-wave plate in front of the cell and an analyzer before the spectrometer are installed on the setup. The polarization measurements consist in acquiring the vertically polarized harmonic intensity emitted at right angle while the linear polarization of the incoming beam is rotated from its vertical to horizontal orientation. The incident fundamental and the scattered harmonic beams being within a horizontal plane, the horizontal polarization of the light is defined from this plane.

3. Results and discussions

The polarization plots measured for $[C_2C_1im][NTf_2]$, $[C_4C_1im][NTf_2]$ and $[C_{10}C_1im][NTf_2]$ are shown in Fig. 1. Similar plots were obtained for $[C_6C_1im][NTf_2]$ and $[C_8C_1im][NTf_2]$, see Fig. S3 in Supporting Information.

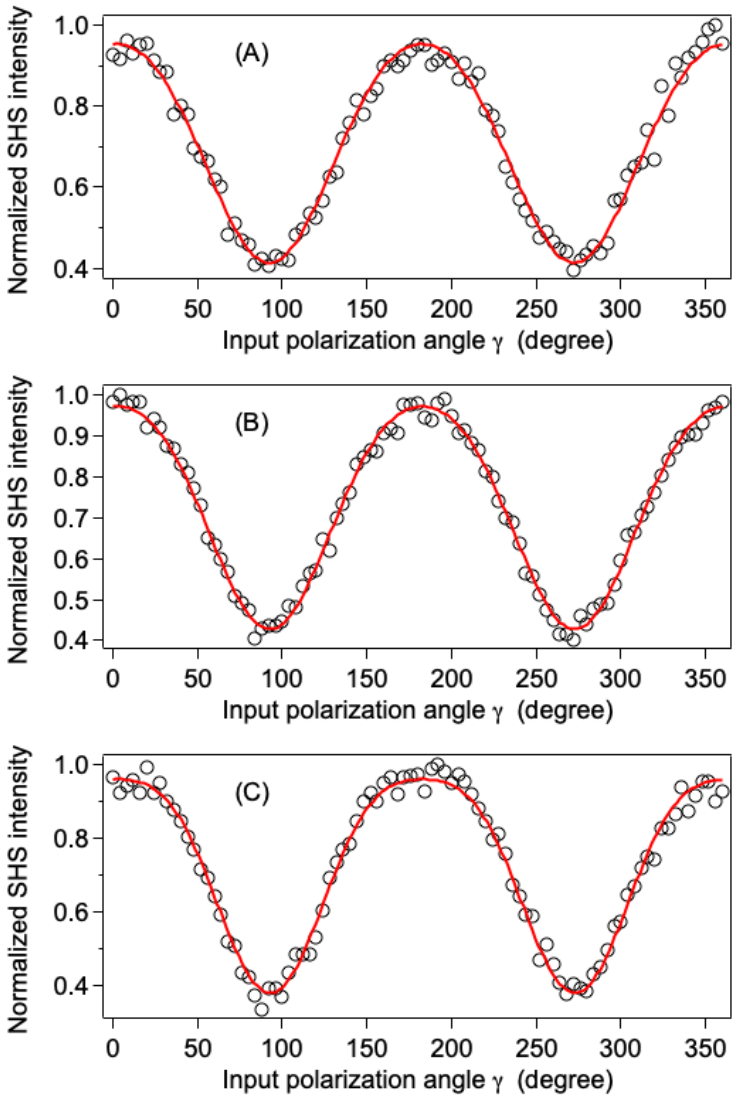

Fig. 1 : Normalized vertically-polarized SHS intensity as a function of the input polarization angle γ for (A): $[C_2C_1im][NTf_2]$, (B): $[C_4C_1im][NTf_2]$ and (C): $[C_{10}C_1im][NTf_2]$.The red line is the plot of the function defined in Eq.4.

All these plots exhibit a similar two-peak pattern. The intensity at the input vertical polarization angle ($\gamma = 0°$) corresponds to the linearly polarized harmonic scattered light in the vertical-vertical geometry, namely I_{VV} intensity. The intensity at the input horizontal polarization angle ($\gamma = 90°$) is labelled I_{HV}. These two intensities can be written as a function

of the hyperpolarizability tensor elements β_{IJK} expressed in the laboratory frame. I_{VV} is thus proportional to $\langle\beta^2_{XXX}\rangle$ and I_{HV} to $\langle\beta^2_{XYY}\rangle$ where the X axis corresponds to the vertical polarization of the fundamental light in the laboratory frame whereas the Y-direction corresponds to the horizontal polarization. The brackets stand for an orientational average owing to the isotropy of the liquid phase. The depolarization ratio *D* can be directly determined from the I_{VV} and I_{HV} SHS intensities and is thus linked to the hyperpolarizability elements as follows [19,55]

$$D = \frac{I_{HV}}{I_{VV}} = \frac{\langle\beta^2_{XYY}\rangle}{\langle\beta^2_{XXX}\rangle} \quad (1)$$

The experimentally determined depolarization ratios *D* do not depend on the chain length within experimental errors. These ratios are reported in Fig. 2. *D* is approximately constant and equal to (0.42 ± 0.03). This value is in agreement with previous works on $[C_2C_1im][NTf_2]$ and $[C_4C_1im][NTf_2]$ but extended here to longer chain lengths [19].

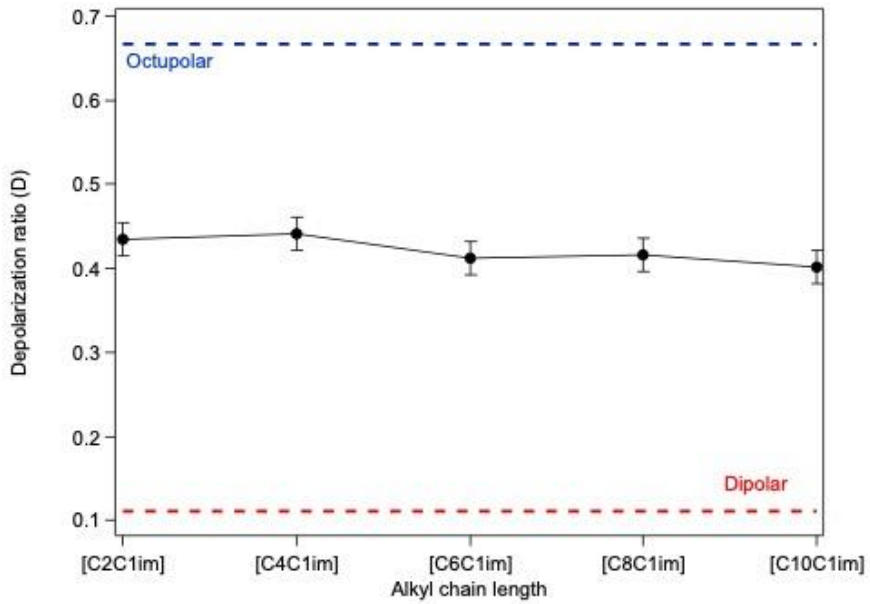

Fig. 2: Depolarization ratio as a function of the alkyl chain length. The values of the depolarization ratio for pure dipolar and pure octupolar systems are reported as red and blue dashed lines respectively.

For low-symmetry structures in liquid phase, it is generally more convenient to use the irreducible spherical representations of the hyperpolarizability β tensor. This permits the use

of the mixed spherical-Cartesian formalism to discuss SHS measurements in terms of multipolar components [56]. Using this formalism allows the β tensor, a symmetric rank-3 tensor, to be decomposed as the irreducible sum of a dipolar (J = 1) and an octupolar (J = 3) tensorial β_J component. The depolarization ratio varies between the value of a pure octupole-like structure (D=2/3) and that of a pure dipolar-like structure (D=1/9). In the case of the present ILs, the depolarization ratios all have an intermediate value as shown in Fig. 2.

The anisotropy parameter $\rho = |\beta_{J=3}|/|\beta_{J=1}|$ compares the relative contributions of the octupolar and dipolar components to the hyperpolarizability tensor β. This parameter is related to the depolarization ratio through [19]:

$$D = \frac{1+\frac{12}{7}\rho^2}{9\left(1+\frac{2}{7}\rho^2\right)} \quad (2)$$

The anisotropy parameter can be deduced from equation Eq.(2), permitting to determine the relative contributions of the octupolar components to the hyperpolarizability tensor with:

$$\phi(\beta_{J=3}) = \rho/(1+\rho) \quad (3)$$

The $\phi(\beta_{J=3})$ contribution for the different ILs is equal to (0.68 ± 0.02) indicating that the SHS response is dominated by an octupolar contribution. This result is in very good agreement with Rodriguez *et al.* who interpreted with DFT calculations the octupolar character of the hyperpolarizability from the local microscopic structures involving at least a double ion pair [19]. In our measurements, the constant value of $\phi(\beta_{J=3})$ indicates that the symmetry is unaffected by the alkyl chain length.

To obtain information on the long-range liquid structuration from the polarization plots of Fig. 1, these data were analysed as a Fourier series[48]:

$$I_{SHS}(\gamma) = i_0 + i_2 cos(2\gamma) + i_4\, cos(4\gamma) \quad (4)$$

where i_0, i_2 and i_4 are the amplitudes of the constant, the harmonic 2γ and the harmonic 4γ terms. In Eq.(4), the parameters i_0 and i_2 are related to the local microscopic structure, i.e. the first hyperpolarizability and i_4 to the long-range correlations [48] In the case of randomly oriented species, SHS is a purely incoherent phenomenon and the amplitude i_4 vanishes [48]. On the contrary, when molecular orientations are correlated, the scattered photons have well-defined phase relationship and i_4 differs from 0.

From the polarization plots of Fig. 1, the constant intensity i_0 and the intensity i_2 at frequency 2γ were subtracted in order to only exhibit the residue at frequency 4γ. The corresponding residue plots at frequency 4γ are provided in Fig. 3. The data for $[C_6C_1im][NTf_2]$ and $[C_8C_1im][NTf_2]$ are given in Supporting Information, see Fig. S3, and are very similar to those of $[C_{10}C_1im][NTf_2]$.

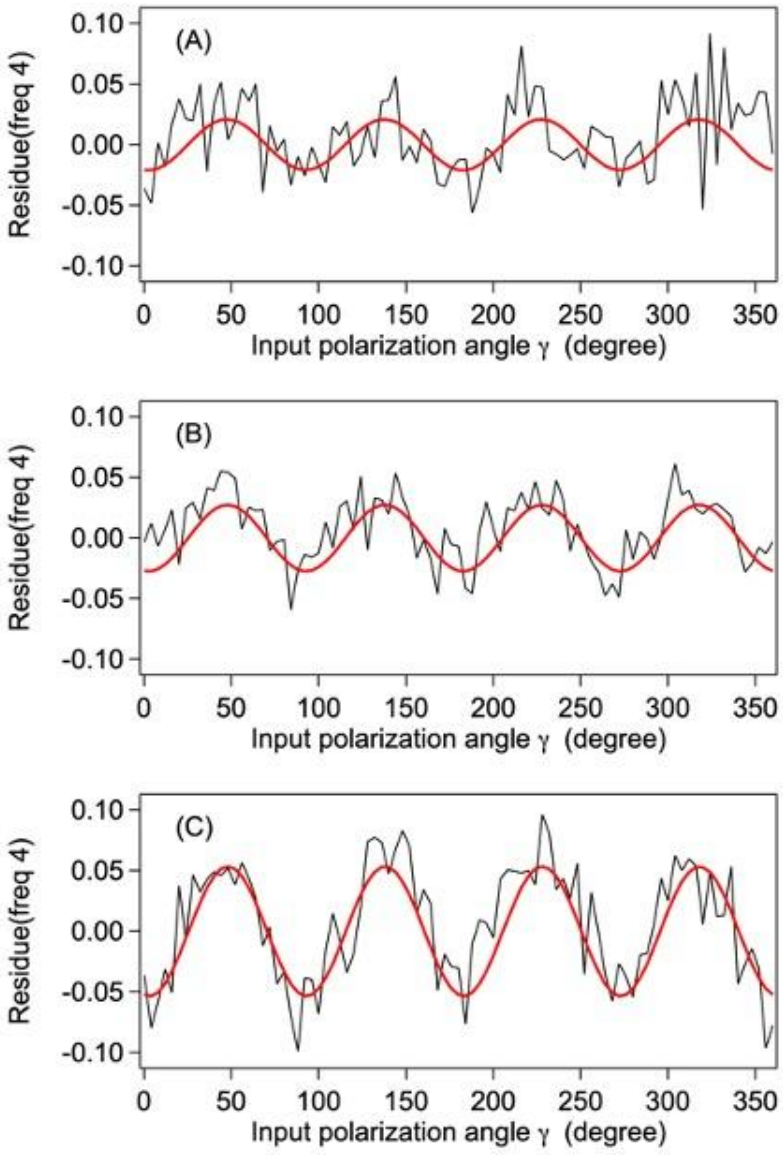

Fig. 3: Residue at the harmonic 4γ of the polarization resolved SH intensity for (A): $[C_2C_1im][NTf_2]$, (B): $[C_4C_1im][NTf2]$ and (C): $[C_{10}C_1im][NTf_2]$. The red lines are the plots of $i_4\ cos(4\gamma)$.

All these plots show a clear oscillation at frequency 4γ indicating that i_4 has a non-vanishing value. It is therefore concluded that orientational correlations are present in the bulk phase of these ILs, even for the shortest alkyl chains. Moreover, it is clear on Fig. 3 that the residue at the harmonic 4γ is not constant with the alkyl chain length.

To study the increase of the i_4 amplitude, we introduced a normalized parameter defined by $I_4 = i_4/i_0$. The 4γ-frequency amplitude can be either positive or negative. This change of

sign is linked to the spatial orientational structuration. Indeed, this parameter is positive, $I_4 \approx 3x10^{-2}$ in the case of pure water whereas it decreases to $I_4 \approx -1x10^{-2}$ at salt concentration close to 1M [48], evidencing a change of the interactions that drive the orientational correlation. In the case of $[C_nC_1im][NTf_2]$ ILs, Fig. 4 shows that the sign of parameter I_4 does not change with *n*. This parameter is always negative and decreases significantly with *n* with an abrupt transition between two regimes between n=4 and 6. For the short alkyl chains, its value is $I_4 \approx -3 \times 10^{-2}$ whereas for the long alkyl chains its value reaches $I_4 \approx -7 \times 10^{-2}$. The transition occurring between *n*=4 and *n*=6 may also be the reinforcement of the alkyl chain steric potential with subsequent saturation effect at largest chain lengths *n*=10.

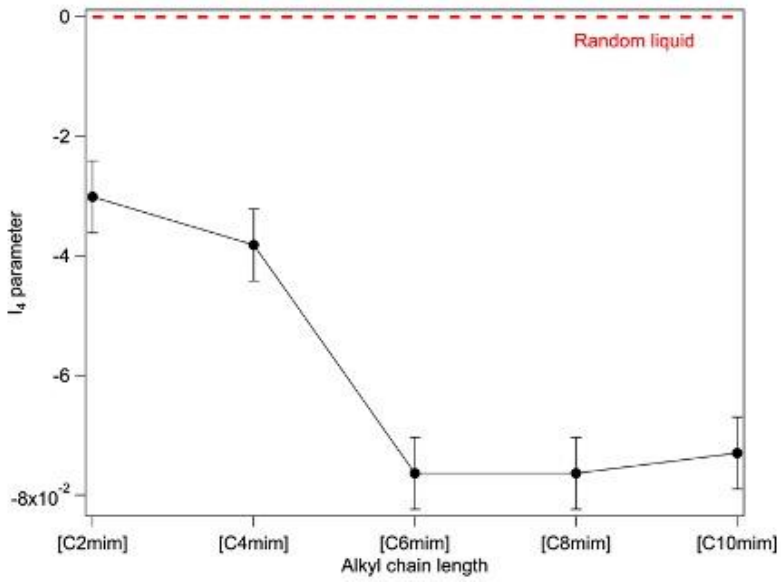

Fig. 4: Experimental I_4 parameter as a function of the alkyl chain length.

In order to interpret the evolution of this parameter I_4 with the alkyl chain length, we use the analytical model recently developed for polarization-resolved SHS intensity to describe the orientational organization of water [48] (details can be found in Supporting Information). In the case of $[C_nC_1im][NTf_2]$ ILs, it can be assumed that the main contribution to the SHS intensity is provided by the imidazolium cation, stemming from the aromatic heterocycle. The relative values of the hyperpolarizability tensor elements at the microscopic scale are obtained

through the value of the depolarization ratio previously defined. Then, the resulting hyperpolarizability at a mesoscopic scale is calculated by summing all the microscopic hyperpolarizabilities within a defined volume, accounting for the different orientations and correlation length r. In this work, we assumed a radial distribution of the different nonlinear sources where all these sources point towards a unique centre. This choice is motivated by the fact that this distribution corresponds to a micelle-like geometry which is justified for amphiphilic systems such as imidazolium salts [57]. In addition, this choice is also motivated by the fact that this distribution gives a negative I4 compared to other distributions such as the azimuthal or polar distributions, as expected from experiments. Finally, to account for the ILs isotropy, global orientational averaging is performed. The resulting I_4 parameter as a function of the distance r is reported in Fig. 5.

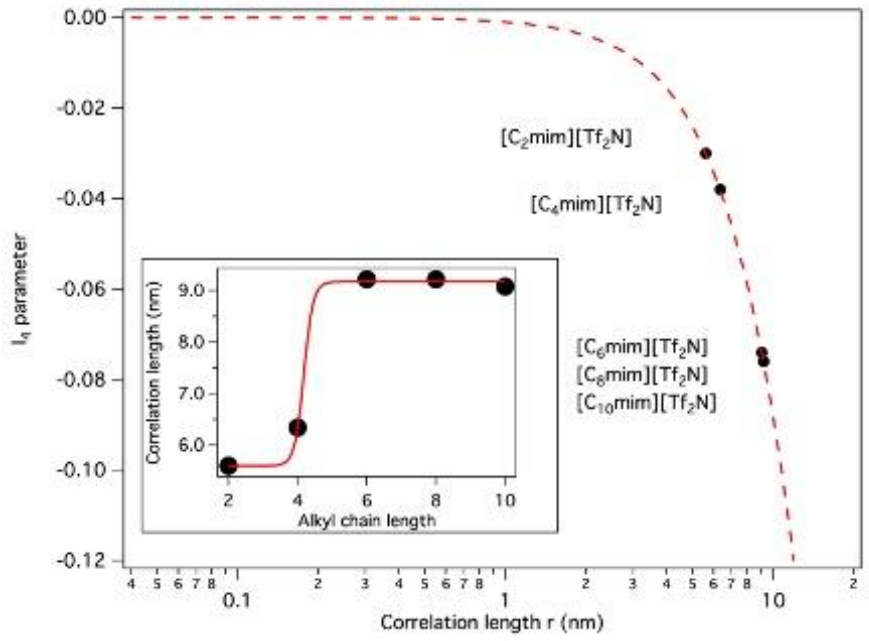

Fig. 5: Calculated I_4 parameter as a function of the correlation length. The experimental values of this parameter for the different ILs are reported in the plot. Inset: Extracted correlation length with the alkyl chain length (the line is a guide to the eye).

This figure exhibits a rapid decrease of I_4 with longer correlation lengths. With this model, the decrease of the I_4 parameter observed in Fig. 4 is associated to an increase of the correlation

length r. This correlation length is in turn plotted for the different ILs as a function of the alkyl chain length, see inset of Fig. 5. An abrupt transition is clearly shown. For shorter alkyl chains, a correlation length between 5 to 6 nm is deduced, signature of a non-random organization at the molecular level in these ILs. For n≥ 6, the correlation length is larger, constant and equal to about 9 nm. In comparison, SWAXS experiments reported in the literature have shown that the characteristic size of nanoscale heterogeneity varies linearly with the alkyl chain length n, in the range 1.5 – 2.5 nm [25]. This was deduced from the peak centered around 2-3 nm^{-1} in the SWAXS data for the longer alkyl chain length ($n \geq 6$). For shorter alkyl chain length, the emergence of this peak being hidden by the tail of a second peak centered around 8-9 nm^{-1}, the linear trend was only extrapolated. It was then deduced that a nanoscale segregation of alkyl chains into nonpolar domains, and of the polar ionic moieties into polar domains. Such segregation seems to begin for $n \geq 3\ or\ 4$. MD calculations have also shown the existence of such segregation. Recently, MD has been used to finely analyze SWAXS experiments showing that the structural transition occurs for $n \geq 5$, from which a percolation regime appears [40]. More precisely, it has been demonstrated that for the smaller alkyl chain lengths (n=2 and 4), the nonpolar aggregates form elongated clusters that become more oblate around n=5 and start to percolate for the longer alkyl chain length. The linear trend reported in SWAXS experiments is not observed in the present SHS data. Moreover, the correlation lengths deduced from the SHS data cannot be directly associated with the dimensions observed in SWAXS experiments. Nevertheless, the transition observed in the correlation length from 5 to 9 nm occurs in the same chain length as the appearance of the percolation regime.

4. Conclusion

In summary, SHS measurements were performed on the 1- Alkyl-3-MethylimidazoliumBis(trifluoromethylsulfonyl)imide IL homologous series $[C_nC_1im][NTf_2]$ ILs with n=2,4,6,8 and 10. Polarization-resolved analysis of the SHS intensity reveals the dominant octupolar nature of the molecular SH response of ILs at all alky chain lengths. Orientational correlations at the nanometer scale are also extracted from the polarization-resolved SHS intensities. These correlations are interpreted as stemming from the radial distribution of the alkyl chains, even for the ILs with the shortest alkyl chains. An abrupt transition to longer correlation distances is observed from the hexyl chain onwards, revealing a clear structural transition. The SHS technique therefore provides a direct observation of structural transition in liquids at scales well-below the diffraction limit and these findings open new interesting perspectives in the future.

Acknowledgements

The authors thank the financial support of the French National Agency for Research under project PROfILE (ANR-17-CE29-0009). The financial support from the Research Federation André Marie Ampère (FRAMA) is also acknowledged.

References

[1] P.G. Jessop, Fundamental properties and practical applications of ionic liquids: concluding remarks, Faraday Discuss. 206 (2018) 587–601.

[2] T.D. Ho, C. Zhang, L.W. Hantao, J.L. Anderson, Ionic Liquids in Analytical Chemistry: Fundamentals, Advances, and Perspectives, Anal. Chem. 86 (2014) 262–285.

[3] T. Welton, Ionic liquids in catalysis, Coord Chem. Rev. 248 (2004) 2459–2477.

[4] S.K. Singh, A.W. Savoy, Ionic liquids synthesis and applications: An overview, J. Mol. Liq. 297 (2020) 112038.

[5] R.L. Vekariya, A review of ionic liquids: Applications towards catalytic organic transformations, J. Mol. Liq. 227 (2017) 44–60.

[6] R. Costa, I.V. Voroshylova, M.N.D.S. Cordeiro, C.M. Pereira, A.F. Silva, Enhancement of differential double layer capacitance and charge accumulation by tuning the composition of ionic liquids mixtures, Electrochim. Acta. 261 (2018) 214–220.

[7] M. Watanabe, M.L. Thomas, S. Zhang, K. Ueno, T. Yasuda, K. Dokko, Application of Ionic Liquids to Energy Storage and Conversion Materials and Devices, Chem. Rev. 117 (2017) 7190–7239.

[8] K. Palunas, K.G. Sprenger, T. Weidner, J. Pfaendtner, Effect of an ionic liquid/air Interface on the structure and dynamics of amphiphilic peptides, J. Mol. Liq. 236 (2017) 404–413.

[9] R. Hayes, G.G. Warr, R. Atkin, Structure and Nanostructure in Ionic Liquids, Chem. Rev. 115 (2015) 6357–6426.

[10] T. Welton, Ionic liquids: a brief history, Biophys. Rev. 10 (2018) 691–706.

[11] K. Dong, X. Liu, H. Dong, X. Zhang, S. Zhang, Multiscale Studies on Ionic Liquids, Chem. Rev. 117 (2017) 6636−6695.

[12] J.K. Konieczny, B. Szefczyk, Structure of Alkylimidazolium-Based Ionic Liquids at the Interface with Vacuum and Water—A Molecular Dynamics Study, J. Phys. Chem. B. 119 (2015) 3795–3807.

[13] J.N.A. Canongia Lopes, A.A.H. Pádua, Nanostructural Organization in Ionic Liquids, J. Phys. Chem. B. 110 (2006) 3330–3335.

[14] R. Costa, C.M. Pereira, A.F. Silva, P.-F. Brevet, E. Benichou, Ordering and Nonideality of Air−Ionic Liquid Interfaces in Surface Second Harmonic Generation, J. Phys. Chem. B. 124 (2020) 3954−3961.

[15] M. Mezger, B.M. Ocko, H. Reichert, M. Deutsch, Surface layering and melting in an ionic liquid studied by resonant soft X-ray reflectivity, Proc Natl Acad Sci U S A. 110 (2013) 3733–3737.

[16] J. Haddad, D. Pontoni, B.M. Murphy, S. Festersen, B. Runge, O.M. Magnussen, et al., Surface structure evolution in a homologous series of ionic liquids, Proc Natl Acad Sci U S A. 115 (2018) E1100–E1107.

[17] P.A. Hunt, B. Kirchner, T. Welton, Characterising the Electronic Structure of Ionic Liquids: An Examination of the 1-Butyl-3-Methylimidazolium Chloride Ion Pair, Chem. Eur. J. 12 (2006) 6762–6775.

[18] T. Köddermann, C. Wertz, A. Heintz, R. Ludwig, Ion-Pair Formation in the Ionic Liquid 1-Ethyl-3-methylimidazolium Bis(triflyl)imide as a Function of Temperature and Concentration, ChemPhysChem. 7 (2006) 1944–1949.

[19] V. Rodriguez, J. Grondin, F. Adamietz, Y. Danten, Local Structure in Ionic Liquids Investigated by Hyper-Rayleigh Scattering, J. Phys. Chem. B. 114 (2010) 15057–15065.

[20] H.K. Kashyap, C.S. Santos, H.V.R. Annapureddy, N.S. Murthy, C.J. Margulis, E.W. Castner Jr, Temperature-dependent structure of ionic liquids: X-ray scattering and simulations, Faraday Discuss. 154 (2012) 133–143.
[21] S. Shigeto, H.-O. Hamaguchi, Evidence for mesoscopic local structures in ionic liquids: CARS signal spatial distribution of Cnmim[PF6] (n=4,6,8), Chem. Phys. Lett. 427 (2006) 329–332.
[22] A. Triolo, A. Mandanici, O. Russina, V. Rodriguez-Mora, M. Cutroni, C. Hardacre, et al., Thermodynamics, Structure, and Dynamics in Room Temperature Ionic Liquids: The Case of 1-Butyl-3-methyl Imidazolium Hexafluorophosphate ([bmim][PF_6]), J. Phys. Chem. B. 110 (2006) 21357–21364.
[23] O. Russina, A. Triolo, L. Gontrani, R. Caminiti, D. Xiao, L.G. Hines Jr, et al., Morphology and intermolecular dynamics of 1-alkyl-3-methylimidazolium bis{(trifluoromethane)sulfonyl}amide ionic liquids: structural and dynamic evidence of nanoscale segregation, J. Phys.: Condens. Matter. 21 (2009) 424121–10.
[24] K. Fujii, S. Kohara, Y. Umebayashi, Relationship between low-Q peak and long-range ordering of ionic liquids revealed by high-energy X-ray total scattering, Phys. Chem. Chem. Phys. 17 (2015) 17838–17843.
[25] D. Pontoni, J. Haddad, M. Di Michiel, M. Deutsch, Self-segregated nanostructure in room temperature ionic liquids, Soft Matter. 13 (2017) 6947–6955.
[26] J. De Roche, C.M. Gordon, C.T. Imrie, M.D. Ingram, A.R. Kennedy, F.L. Celso, et al., Application of Complementary Experimental Techniques to Characterization of the Phase Behavior of [C, Chem. Mater. 15 (2003) 3089–3097.
[27] K. Fujii, R. Kanzaki, T. Takamuku, Y. Kameda, S. Kohara, M. Kanakubo, et al., Experimental evidences for molecular origin of low- Qpeak in neutron/x-ray scattering of 1-alkyl-3-methylimidazolium bis(trifluoromethanesulfonyl)amide ionic liquids, J. Chem. Phys. 135 (2011) 244502–12.
[28] C. Hardacre, J.D. Holbrey, C.L. Mullan, T.G.A. Youngs, D.T. Bowron, Small angle neutron scattering from 1-alkyl-3-methylimidazolium hexafluorophosphate ionic liquids ([Cnmim][PF6], n=4, 6, and 8), J. Chem. Phys. 133 (2010) 074510–8.
[29] R. Hayes, S. Imberti, G.G. Warr, Atkin, Effect of Cation Alkyl Chain Length and Anion Type on Protic Ionic Liquid Nanostructure, J. Phys. Chem. C. 118 (2014) 13998−14008.
[30] V. Mazan, M. Boltoeva, Insight into the ionic interactions in neat ionic liquids by Diffusion Ordered Spectroscopy Nuclear Magnetic Resonance, J. Mol. Liq. 240 (2017) 74–79.
[31] B. Hyun, S.V. Dzyuba, R.A. Bartsch, E.L.J. Quitevis, Intermolecular Dynamics of Room-Temperature Ionic Liquids: Femtosecond Optical Kerr Effect Measurements on 1-Alkyl-3-methylimidazolium Bis((trifluoromethyl)sulfonyl)imides, J. Phys. Chem. A. 106 (2002) 7579–7585.
[32] K. Yamamoto, M. Tani, M. Hangyo, Terahertz Time-Domain Spectroscopy of Imidazolium Ionic Liquids, J. Phys. Chem. B. 111 (2007) 4854–4859.
[33] N.T. Hunt, A.A. Jaye, S.R. Meech, Ultrafast dynamics in complex fluids observed through the ultrafast optically-heterodyne-detected optical-Kerr-effect (OHD-OKE), Phys. Chem. Chem. Phys. 9 (2007) 2167–2180.
[34] D. Xiao, L.G. Hines, R.A. Bartsch, E.L. Quitevis, Intermolecular Vibrational Motions of Solute Molecules Confined in Nonpolar Domains of Ionic Liquids, J. Phys. Chem. B. 113 (2009) 4544–4548.

[35] S. Schrödle, G. Annat, D.R. MacFarlane, M. Forsyth, R. Buchner, G. Hefter, Broadband dielectric response of the ionic liquid N-methyl-N-ethylpyrrolidinium dicyanamide, Chem. Commun. 99 (2006) 1748–1750.
[36] H. Weingärtner, P. Sasisanker, C. Daguenet, P.J. Dyson, I. Krossing, J.M. Slattery, et al., The Dielectric Response of Room-Temperature Ionic Liquids: Effect of Cation Variation, J. Phys. Chem. B. 111 (2007) 4775–4780.
[37] K. Iwata, H. Okajima, S. Saha, H.-O. Hamaguchi, Local Structure Formation in Alkyl-imidazolium-Based Ionic Liquids as Revealed by Linear and Nonlinear Raman Spectroscopy, Acc. Chem. Res. 40 (2007) 1174–1181.
[38] E.W. Castner, J.F. Wishart, H. Shirota, Intermolecular Dynamics, Interactions, and Solvation in Ionic Liquids, Acc. Chem. Res. 40 (2007) 1217–1227.
[39] R. Clark, M.A. Nawawi, A. Dobre, D. Pugh, Q. Liu, A.P. Ivanov, et al., The effect of structural heterogeneity upon the microviscosity of ionic liquids, Chem. Sci. 11 (2020) 6121–6133.
[40] A.A.H. Padua, M.F. Costa Gomes, J.N.A. Canongia Lopes, Molecular Solutes in Ionic Liquids: A Structural Perspective, Acc. Chem. Res. 40 (2007) 1087–1096.
[41] J.N.C. Lopes, M.F.C. Gomes, A.A.H. Pádua, Nonpolar, Polar, and Associating Solutes in Ionic Liquids, J. Phys. Chem. B. 110 (2006) 16816–16818.
[42] K. Shimizu, C.E.S. Bernardes, J.N. Canongia Lopes, Structure and Aggregation in the 1-Alkyl-3-Methylimidazolium Bis(trifluoromethylsulfonyl)imide Ionic Liquid Homologous Series, J. Phys. Chem. B. 118 (2014) 567–576.
[43] J.C. Araque, J.J. Hettige, C.J. Margulis, Modern Room Temperature Ionic Liquids, a Simple Guide to Understanding Their Structure and How It May Relate to Dynamics, J. Phys. Chem. B. 119 (2015) 12727−12740.
[44] B.L. Bhargava, M.L. Klein, Molecular Dynamics Studies of Cation Aggregation in the Room Temperature Ionic Liquid [C10mim][Br] in Aqueous Solution, J. Phys. Chem. A. 113 (2009) 1898–1904.
[45] G.C. Gschwend, A. Olaya, H.H. Girault, How to polarise an interface with ions: the discrete Helmholtz model, Chem. Sci. 13 (2020) 73–7.
[46] G.C. Gschwend, M. Kazmierczak, A.J. Olaya, P.-F. Brevet, H.H. Girault, Two dimensional diffusion-controlled triplet–triplet annihilation kinetics, Chem. Sci. 10 (2019) 7633–7640.
[47] P. Kaatz, Collision induced hyper-Rayleigh light scattering in CCl4, Molecular Physics. 88 (1996) 683–692.
[48] J. Duboisset, P.-F. Brevet, Salt-induced Long-to-Short Range Orientational Transition in Water, Phys. Rev. Lett. 120 (2018) 263001.
[49] J. Zyss, T.C. Van, C. Dhenaut, I. Ledoux, Harmonic Rayleigh scattering from nonlinear octupolar molecular media: the case of crystal violet, Chemical Physics. 177 (1993) 281–296.
[50] I. López-Duarte, J.E. Reeve, J. Pérez-Moreno, I. Boczarow, G. Depotter, J. Fleischhauer, et al., "Push-no-pull" porphyrins for second harmonic generation imaging, Chem. Sci. 4 (2013) 2024–4.
[51] G. Revillod, N. Nishi, T. Kakiuchi, Orientation Correlation of Sulfosuccinate-based Room-Temperature Ionic Liquids Studied by Polarization-Resolved Hyper-Rayleigh Scattering, J. Phys. Chem. B. 113 (2009) 15322–15326.
[52] F. Castet, E. Bogdan, A. Plaquet, L. Ducasse, B. Champagne, V. Rodriguez, Reference molecules for nonlinear optics: A joint experimental and theoretical investigation, J. Chem. Phys. 136 (2012) 024506–16.

[53] G. Revillod, J. Duboisset, I. Russier-Antoine, E. Benichou, G. Bachelier, C. Jonin, et al., Multipolar Contributions to the Second Harmonic Response from Mixed DiA−SDS Molecular Aggregates, J. Phys. Chem. C. 112 (2008) 2716–2723.
[54] A. Deniset-Besseau, J. Duboisset, E. Benichou, F. Hache, P.-F. Brevet, M.-C. Schanne-Klein, Measurement of the Second-Order Hyperpolarizability of the Collagen Triple Helix and Determination of Its Physical Origin, J. Phys. Chem. B. 113 (2009) 13437–13445
[55] S. Brasselet, J. Zyss, Multipolar molecules and multipolar fields: probing and controlling the tensorial nature of nonlinear molecular media, J. Opt. Soc. Am. B. 15 (1998) 257–288.
[56] J. Zyss, I. Ledoux, Nonlinear optics in multipolar media: theory and experiments, Chem. Rev. 94 (1994) 77–105.
[57] J. Bowers, C. P. Butts, P. J. Martin, M. C. Vergara-Guterriez, Aggregation behavior of aqueous solutions of ionic liquids, Langmuir 20 (2004) 2191-2198.